0026-895X/11/8002-345–355$25.00
MOLECULAR PHARMACOLOGY
Copyright © 2011 The American Society for Pharmacology and Experimental Therapeutics
Mol Pharmacol 80:345–355, 2011

Vol. 80, No. 2
72405/3701348
Printed in U.S.A.

Heteropoda Toxin 2 Interaction with Kv4.3 and Kv4.1 Reveals Differences in Gating Modification

Christopher V. DeSimone,[1] Vladislav V. Zarayskiy,[2] Vladimir E. Bondarenko[3] and Michael J. Morales

Department of Physiology & Biophysics, University at Buffalo, the State University of New York, Buffalo, New York

Received March 22, 2011; accepted April 26, 2011

ABSTRACT

Kv4 (*Shal*) potassium channels are responsible for the transient outward K^+ currents in mammalian hearts and central nervous systems. Heteropoda toxin 2 (HpTx2) is an inhibitor cysteine knot peptide toxin specific for Kv4 channels that inhibits gating of Kv4.3 in the voltage-dependent manner typical for this type of toxin. HpTx2 interacts with four independent binding sites containing two conserved hydrophobic amino acids in the S3b transmembrane segments of Kv4.3 and the closely related Kv4.1. Despite these similarities, HpTx2 interaction with Kv4.1 is considerably less voltage-dependent, has smaller shifts in the voltage-dependences of conductance and steady-state inactivation, and a 3-fold higher K_d value. Swapping four nonconserved amino acids in S3b between the two channels exchanges the phenotypic response to HpTx2. To understand these differences in gating modification, we constructed Markov models of Kv4.3 and Kv4.1 activation gating in the presence of HpTx2. Both models feature a series of voltage-dependent steps leading to a final voltage-independent transition to the open state and closely replicate the experimental data. Interaction with HpTx2 increases the energy barrier for channel opening by slowing activation and accelerating deactivation. The greater degree of voltage-dependence in Kv4.3 occurs because it is the voltage-dependent transitions that are most affected by HpTx2; in contrast, it is the voltage-independent step in Kv4.1 that is most affected by the presence of toxin. These data demonstrate the basis for subtype-specificity of HpTx2 and point the way to a general model of gating modifier toxin interaction with voltage-gated ion channels.

Introduction

Potassium currents with fast activation and inactivation kinetics are present in many mammalian tissues and are often conducted by the three members of the *Shal* (Kv4) family of voltage-gated K^+ channels (Birnbaum et al., 2004). These channels are best known for their key roles in cardiovascular and nervous systems. Kv4.2 and Kv4.3 are the pore-forming channel subunits of the fast-recovering cardiac transient outward current that is most prominently found in the atria, right ventricle, and left ventricular epicardium of many mammals, in which their prominent role in early repolarization influences calcium current magnitude and myocardial contractility (Nerbonne and Kass, 2005). In neurons, they are responsible for the I_A K^+ current in the somatodendritic region, which limits the amplitude and accelerates the decay of excitatory postsynaptic action potentials and inhibits back propagation of depolarization in dendrites (Covarrubias et al., 2008). A physiological role for the third member of the family, Kv4.1, has not been clearly established.

The sequences of the three Kv4 channels are highly conserved: there is 87% sequence identity between voltage sensor and pore domains of Kv4.3 and Kv4.1, and 95% between Kv4.3 and Kv4.2. As expected from channels with this level of conservation, they share many gating properties. In heterologous expression systems, their conductance-voltage relationships are best described by a Boltzmann function with midpoints ($V_{1/2}$) near 0 mV; activation and deactivation are fast compared with most other voltage-gated K^+ channels (Birnbaum et al., 2004). Inactivation of *Shal* channels is a

This work was supported by the American Heart Association Founders and Southeast Affiliates [Scientist Development Grant 0235500T, Predoctoral Fellowship 0615662T, Grant-in-aid 10GRNT4720012]; the John R. Oishei Foundation; and a Georgia State University Brain and Behavior Research Initiation Grant.

This work was presented previously in abstract form at the 55th Annual Meeting of the Biophysical Society; 5–9 Mar 2011; Baltimore, MD (*Biophys J* **100:**283a, Supplement 1), and as a portion of a doctoral thesis: DeSimone CV (2009), HpTx2 gating modification involves distinct amino acids in S3b region of Kv4, the State University of New York at Buffalo.

[1] Current affiliation: Department of Internal Medicine, Mayo Clinic, Rochester, Minnesota.

[2] Current affiliation: Anchor Therapeutics, Cambridge, Massachusetts.

[3] Current affiliation: Department of Mathematics and Statistics, Georgia State University, Atlanta, Georgia.

Article, publication date, and citation information can be found at http://molpharm.aspetjournals.org.

doi:10.1124/mol.111.072405.

ABBREVIATIONS: HpTx2, Heteropoda toxin 2; TMS, transmembrane segment; VSD, voltage-sensor domain; ICK, inhibitor cysteine knot; SSIA, steady-state inactivation; G-V, conductance-voltage.

complex and relatively slow process occurring from multiple open and closed states (Bähring and Covarrubias, 2011).

Potassium currents generated by *Shal* channels in vivo have been identified using the closely related peptide toxins HpTx2 and HpTx3 (Sanguinetti et al., 1997; Brahmajothi et al., 1999; Himmel et al., 1999; Kassiri et al., 2002; Ramakers and Storm, 2002; Varga et al., 2004; Nerbonne et al., 2008; Liu et al., 2011). The best characterized is HpTx2, a 30-amino acid toxin originally purified from the venom of the spider *Heteropoda venatoria* (Sanguinetti et al., 1997). It is one of more than 300 known ion-channel peptide toxins that form an "inhibitor cysteine knot" (ICK) motif, most of which have been identified in spider venom (Gracy et al., 2008). Both in vivo data and our studies using heterologously expressed channels have strongly suggested that HpTx2 is specific for Kv4 channels (Zarayskiy et al., 2005). HpTx2 inhibition of Kv4.3 was voltage-dependent, shifting the threshold for activation to more depolarized potentials, speeding deactivation, and slowing inactivation (Zarayskiy et al., 2005). Alanine scanning mutagenesis showed that HpTx2 interacts with two amino acids in the S3b TMS of the VSD (DeSimone et al., 2009). These characteristics established HpTx2 as a gating modifier toxin that inhibits the channel by interfering with the movement of the voltage sensor domain during gating.

In contrast to Kv4.3, the HpTx2-induced gating modification of Kv4.1 was much less voltage-dependent (Zarayskiy et al., 2005). This surprising observation led us to compare the interaction between HpTx2 and these two channels. In this study, we show that Kv4.1 and Kv4.3 share a binding site for HpTx2 in the S3b TMS, ruling out an entirely different mechanism of gating modification for the two channels. We found that the molecular basis of differences in voltage-dependent inhibition were due to a nonconserved four-amino acid region in S3b adjacent to the toxin's putative binding site. To gain insights into the mechanism responsible for differences in HpTx2 gating modification, we developed Markov models of Kv4.1 and Kv4.3 activation in the presence of HpTx2. In the absence of toxin, we propose five closed states leading to an open state. The transitions between the closed states are voltage-dependent, whereas the transition from the final preopen closed to the open state is voltage-independent. To account for HpTx2 interaction, we added four toxin-bound states and the transition rates to account for experimentally observed toxin-dependent effects. The model suggests that HpTx2 primarily effects the voltage-dependent transitions in Kv4.3, resulting in a high degree of voltage-dependent inhibition by HpTx2. In contrast, the toxin stabilizes the final preopen closed state of Kv4.1. Because this transition is voltage-independent, there is a lower degree of voltage dependence of HpTx2-induced gating modification. These experiments show that subtle differences in the gating properties of two closely related K^+ channels can result in large differences in gating modification by toxins or drugs that have similar molecular basis of interaction with their ion channel targets.

Materials and Methods

Preparation of RNA for Oocyte Injection. The short form of rat Kv4.3 (636 amino acids; National Center for Biotechnology Information accession number NP_113927), and the mouse Kv4.1 (NP_032449) were described previously (Wang et al., 2002; Zarayskiy et al., 2005). Site-directed mutagenesis was performed as described previously (DeSimone et al., 2009); mutant identity was confirmed by DNA sequencing. Plasmids encoding cloned channels were linearized by restriction endonuclease digestion and transcribed using T7 RNA polymerase (mMessage Machine; Ambion, Austin, TX). The reaction was terminated by DNAase I treatment followed by precipitation of RNA with LiCl and suspension in RNAase-free water included in the mMessage Machine kit. The sample concentration was determined by absorbance at 260 nm, adjusted to 500 ng/ml, and stored at −80°C.

***Xenopus laevis* Oocyte Preparation.** Use of *X. laevis* has been considered and approved for numbers of animals, humane treatment, care, and method of euthanasia by the University at Buffalo-SUNY Institutional Animal Care and Use Committee and was carried out in accordance with the Declaration of Helsinki and with the *Guide for the Care and Use of Laboratory Animals* (Institute of Laboratory Animal Resources, 1996) as adopted and promulgated by the U.S. National Institutes of Health (Bethesda, MD).

Oocytes were prepared as described previously (DeSimone et al., 2009). Frogs obtained from Xenopus I (Ann Arbor, MI) were anesthetized by immersion in 2.0 mM 3-aminobenzoic acid ethyl ester (Sigma-Aldrich, St. Louis, MO) for at least 10 min. The ovarian lobes were harvested and placed in Ca^{2+}-free ND96 (96 mM NaCl, 2 mM KCl, 1 mM $MgCl_2$, and 5 mM HEPES, pH 7.4) and treated with 1 to 2 mg/ml collagenase (type II; Sigma-Aldrich) to remove the follicular cell layer. Oocytes were injected with 10 to 50 nl of in vitro-transcribed mRNA. Injected oocytes were incubated at 18°C in normal ND96 (including 1.8 mM $CaCl_2$) plus antibiotic/antimycotic (Invitrogen, Carlsbad, CA) for 3 to 7 days.

Two-Electrode Voltage-Clamp Technique. Currents were measured in oocytes using a two-microelectrode Dagan CA-1B amplifier as described previously (Wang et al., 2004; Wang et al., 2005). Electrodes were filled with 3 M KCl. Experiments were performed at room temperature (20–24°C), or at 16°C where noted, in either ND96 plus 0.1% bovine serum albumin or 98K plus 0.1% bovine serum albumin (98 mM KCl, 1 mM $MgCl_2$, 1.8 mM $CaCl_2$, and 5 mM HEPES, pH 7.4). For experiments performed at 16°C, a Dagan HCC-100 temperature controller was used to regulate both the recording chamber and solution temperatures. Data were digitized at either 50 or 5 kHz using Clampex 9.2 (Molecular Devices, Sunnyvale, CA), and analyzed with Clampfit 9.2, Microsoft Excel 2007 (Microsoft, Redmond, WA), or SigmaPlot 9 (Systat Software, Inc., San Jose, CA). Raw current traces shown were neither leakage- nor capacitance-subtracted.

Pulse Protocols and Data Analysis. The holding potential for all pulse protocols was −90 mV. A two-pulse protocol was used to measure the current-voltage (I-V), conductance-voltage (G-V), steady-state inactivation (SSIA) relationships, and time to peak current. From the holding potential, 3-s voltage steps (P1) were applied from −120 to +50 mV in 10-mV increments followed by a 1-s pulse (P2) to +50 mV, with a 3-s interval before the next P1 pulse. Normalized current (I/I_{max}) was calculated as the ratio of the maximum current during the P1 pulse to the maximum current during the 50-mV P1 pulse before application of HpTx2. Conductance $G(V)$ at each voltage was calculated from the equation $G(V) = I_{max,1}/(V - E_K)$, where V is the depolarization voltage during P1, $I_{max,1}$ is the maximum current during P1, and $E_K = -100$ mV, the reversal potential of K^+ for *X. laevis* oocytes in ND96. The G-V relationship was obtained by fitting $G(V)$, normalized to the maximal conductance value, with a Boltzmann function $f_a(V) = G_{max}/(1 + \exp[(V_{1/2} - V)/k])$, where $V_{1/2}$, k, and G_{max} are the half-activation potential, the slope factor, and 1.0, respectively. Steady-state inactivation was determined as the ratio of the maximum current during P2, $I_{max,2}$ for the P1 depolarization voltage to the maximum value of $I_{max,2}$. The voltage dependence of steady-state inactivation relationships were fitted by the Boltzmann function $f_i(V) = 1/(1 + \exp[(V_{1/2,i} - V)/k_i])$,

where $V_{1/2,i}$ and k_i are the half-inactivation potential and the slope factor, respectively.

Association/dissociation experiments (Figs. 2A and 3, J and K) were performed with a two-pulse protocol: the P1 pulse was to −10 mV for 12 ms, followed by a P2 pulse to −50 mV for 150 ms, with a 1-s interpulse interval. The data represent the normalized reciprocal current amplitude measured from the maximum of the P2 pulse. The on and off rates were fit with the functions $f_{on}(t) = C \times \exp(-t/4\tau_{on})$ and $f_{off}(t) = C \times [(1 - \exp(-t/\tau_{off})]^4$, respectively. The dissociation constant (K_d) = k_{off}/k_{on}, where $k_{off} = 1/\tau_{off}$, and $k_{on} = 1/(4 \times [HpTx2] \times \tau_{on})$.

Activation was measured using a series of 1000-ms pulses from the −90-mV holding potential to a series of steps from −30 to +50 mV in 10-mV increments. The activation time constants were determined by fitting the activation time course to the function $f_{act}(t) = C \times (1 - \exp[-t/\tau_{act}])^4$. To measure deactivation, the P1 pulse was set to +50 mV for 12 ms, followed by a 150-ms P2 pulse from −120 to −40 mV in 10-mV increments. Deactivation time constants were determined by fitting the currents in the P2 pulse to the function $f_{deact}(t) = C \times (1 - \exp[-t/\tau_{deact}])$.

Model Development. Model development was performed on a DEC Alpha workstation using Fortran 90. The Markov model was implemented as a set of evolution differential equations for five closed states, C_0 to C_4, and one open state, O. The numerical solution of differential equations was performed by a fourth-order Runge-Kutta method. Channel models were allowed to run for at least 600 s to calculate the steady-state values of occupancies of channel states and were used as the initial conditions (Wang et al., 2004).

Results

Gating Modification of Kv4.1 by HpTx2. Peptide toxins have found wide use as structural probes for ion channels and as pharmaceutical agents (Lewis and Garcia, 2003; Catterall et al., 2007; Estrada et al., 2007; Swartz, 2007; Hodgson and Isbister, 2009; Dutertre and Lewis, 2010). Their interaction with ion channels falls into two general classes: pore blockade, or gating modification. Pore-blocking toxins bind to the pore region of a channel and prevent permeation of ions through occlusion of the external channel pore. Gating modifier toxins inhibit or activate ion channel conductance by interfering with the energetics of channel gating (Catterall et al., 2007; Swartz, 2007).

A hallmark of gating modifier toxin activity on voltage-gated K^+ channels is voltage-dependent inhibition; there is a greater degree of channel inhibition at voltages near the activation threshold (Swartz and MacKinnon, 1995). This effect can be seen by comparing the I-V relationships of Kv4.3 in the presence and absence of 2 μM HpTx2 (Fig. 1A). Note that at voltages less than 0 mV, there is a much greater degree of channel inhibition than at higher voltages, indicating strong voltage-dependent inhibition. Kv4.1 is a close relative of Kv4.3, with more than 90% amino acid identity from the beginning of S1 to the end of S6. However, inhibition of Kv4.1 by HpTx2 exhibited less voltage dependence (Fig. 1B). For example, at 0 mV, 80% of the Kv4.3 current is inhibited, whereas Kv4.1 current is only reduced by half. In contrast, at +50 mV, 2 μM HpTx2 inhibits both channels to nearly the same degree: 38% of Kv4.3 current is inhibited versus 36% of the Kv4.1 current (Fig. 1, A–D). This manifests itself in relatively feeble shifts in the normalized G-V relationship when toxin is applied to Kv4.1; the change in voltage at one half-the maximum normalized conductance ($\Delta V_{1/2}$) values are 22.0 ± 1.6 and 10.2 ± 1.2 mV for Kv4.3 and Kv4.1, respectively (Fig. 1, E and F, and Table 1). Similar differences were observed in the voltage dependences of steady-state inactivation, with Kv4.3 having much larger shifts in voltage dependence than Kv4.1 (Fig. 1, G and H, and Table 1).

Kv4.3 and Kv4.1 also showed differences in their apparent affinity for HpTx2. To determine the gating modification kinetics and apparent dissociation constant we used a method described in detail elsewhere (Swartz and MacKinnon, 1997; DeSimone et al., 2009). In brief, we used a two-pulse protocol from our previously determined threshold depolarization voltages of −10 to −50 mV at 1-s intervals. The bath solution contained 98 mM K^+ to ensure sufficiently large tail current amplitudes to accurately measure the toxin occupancy. After establishing baseline current amplitude, toxin was applied directly to the chamber. When toxin inhibition reached steady state, the toxin was washed off the oocyte by perfusion (Fig. 2A). The time courses of association and dissociation were fit with exponential functions; dissociation was fit with a fourth power exponential function to account for the 4-fold symmetry of Kv4.1, which suggests four HpTx2 binding sites, as was established for HpTx2 interaction with Kv4.3 (DeSimone et al., 2009). The K_d of HpTx2 was 7.1 ± 1.1 μM (Table 2), roughly 3-fold higher than the 2.3 ± 0.3 μM concentration of HpTx2 with Kv4.3.

HpTx2 inhibition of Kv4.3 occurs by gating modification through a putative binding site in S3b (DeSimone et al., 2009); however, the relative lack of voltage-dependence observed in the Kv4.1 I-V relationship suggested that HpTx2 might somehow be occluding the pore of this channel. Given the apparent structural similarity between Kv4.1 and Kv4.3, this would probably mean that the channels do not share the same toxin binding site, which in turn would suggest a different mechanism of channel inhibition. We found previously that the critical amino acids necessary for toxin-channel interaction in Kv4.3 were a leucine and valine at positions 275 and 276 (DeSimone et al., 2009). The amino acids at the analogous positions in Kv4.1 are a leucine and a phenylalanine (Fig. 2B). Therefore, we constructed Kv4.1 [(L275,F276)A], substituting the two amino acids at positions 275 and 276 with alanine, similar to the modification that nearly eliminates Kv4.3 interaction with HpTx2 (DeSimone et al., 2009). When expressed in *X. laevis* oocytes, the mutant Kv4.1 expressed currents similar to the wild-type Kv4.1. However, there is almost complete loss of gating modification after application of 5 μM HpTx2 (Fig. 2, C and D, and Table 1). These data show that the putative binding site of HpTx2 is the same in Kv4.3 and Kv4.1, strongly suggesting that the differences in gating modification are due to intrinsic differences in gating between the two channels and not by the location of toxin binding.

Differences in the S3b TMS Account for the Difference in Gating Modification. Although putative binding site differences between Kv4.3 and Kv4.1 do not account for the differences in channel behavior toward HpTx2, other amino acid differences could account for this phenomenon. Aside from the typically nonconserved S1–S2 TMS external linker, the largest stretch of different amino acids in the voltage sensor and pore domains stretches from amino acid Val276 to Asn279 in Kv4.3 and Phe276 to Lys279 in Kv4.1 (Fig. 2B). Proximity to both the apparent HpTx2 binding site on Kv4.3 and the S4 transmembrane voltage-sensing sequence suggested that these amino acids might be important

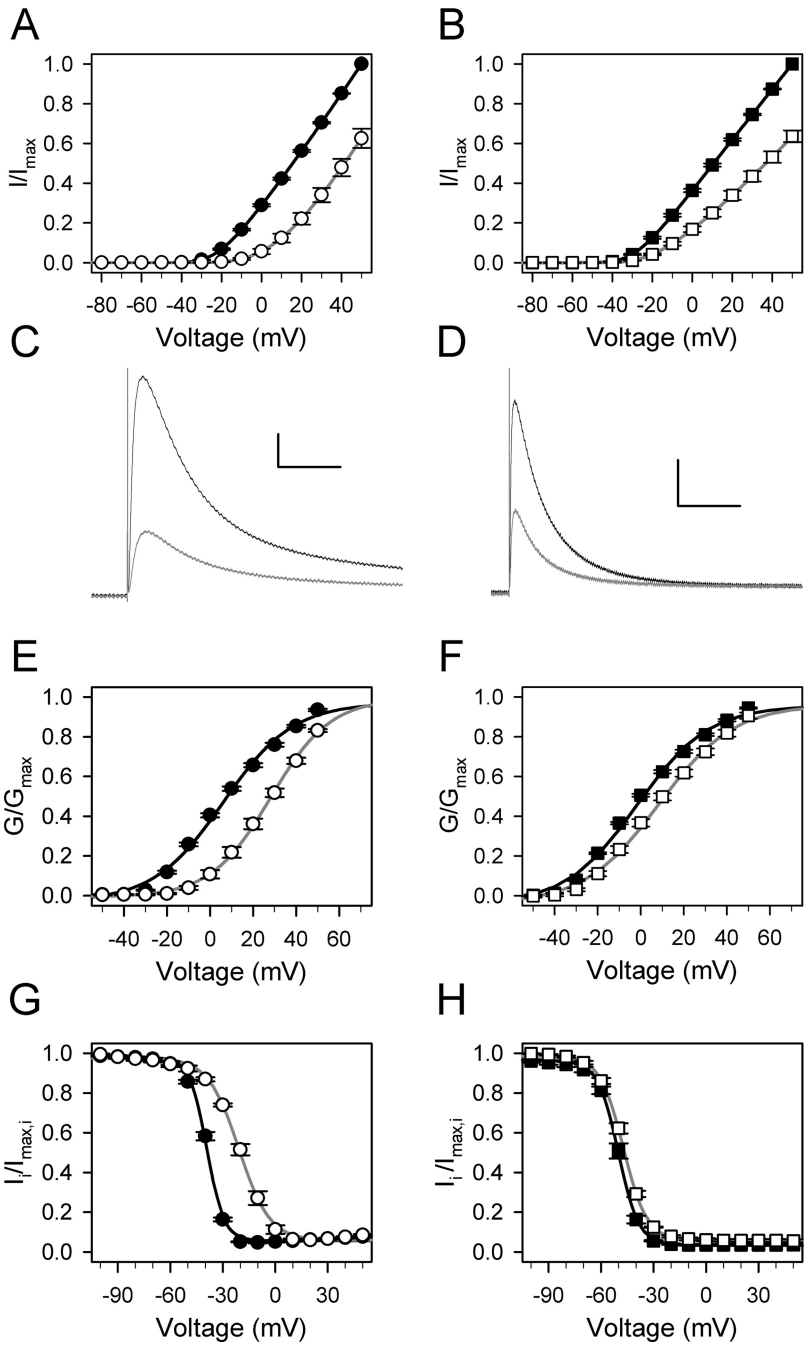

Fig. 1. Kv4.3 and Kv4.1 react differently to the application of 2 μM HpTx2. Plots of Kv4.3 are at left; all plots of Kv4.3 use circles. Kv4.1 is at right; all its plots use squares. Closed symbols with black lines represent the controls, whereas open symbols with gray lines represent the result of HpTx2 application. These conventions are maintained throughout this work. The pulse protocols and fitting algorithms (E–H) are described under *Materials and Methods*. All except for C and D are shown as the mean ± S.E.M., n = 5 to 6. A, current-voltage relationship of Kv4.3 ± HpTx2. B, current-voltage relationship of Kv4.1 ± HpTx2. C and D, representative current traces of Kv4.3 and Kv4.1 in the presence of HpTx2 (gray). Currents were elicited from a holding potential of −90 to 0 mV for 2.5 s. Scale bars, 0.5 μA × 0.5 s. The data were neither leakage- nor capacitance-subtracted. E and F, conductance-voltage relationships of Kv4.3 and Kv4.1 in the presence of HpTx2. G and H, voltage-dependence of steady-state inactivation of Kv4.3 and Kv4.1 in the presence of HpTx2. Note in E and G that Kv4.3 has robust changes in voltage dependence to more depolarized potentials after application of HpTx2, a response characteristic of gating modifier toxins. In contrast, the same concentration of HpTx2 induces relatively feeble voltage-dependent effects in Kv4.1 (see Table 1).

TABLE 1

Influence of HpTx2 on $V_{1/2}$ and k values of steady-state channel properties

All values are given in millivolts as mean ± S.E.M., n = 4 to 6. The [HpTx2] was 2 μM except for Kv4.1[(L275,F276)A] with which 5 μM HpTx2 was used. Kv4.3 conductance values are from DeSimone et al. (2009).

Channel	Conductance				Steady-State Inactivation			
	Control		+HpTx2		Control		+HpTx2	
	$V_{1/2}$	k	$V_{1/2}$	k	$V_{1/2}$	k	$V_{1/2}$	k
Kv4.1	−1.8 ± 0.7	16.4 ± 0.4	8.4 ± 1.0	17.17 ± 0.3	−49.5 ± 0.06	6.0 ± 0.06	−47.2 ± 0.02	6.7 ± 0.02
Kv4.3	6.1 ± 0.7	16.1 ± 0.2	28.1 ± 1.4	13.6 ± 0.6	−39.1 ± 1.0	4.9 ± 0.02	−20.7 ± 1.8	8.8 ± 0.1
Kv4.1 [(L275,F276)A]	4.4 ± 0.7	14.0 ± 0.6	6.1 ± 1.0	13.8 ± 0.7	−48.2 ± 0.3	6.0 ± 0.02	−48.7 ± 0.3	6.7 ± 0.02
Kv4.1 [276VMTN]	0.1 ± 1.0	16.8 ± 0.1	32.2 ± 2.2	16.8 ± 1.7	−49.2 ± 0.02	5.0 ± 0.02	−33.2 ± 0.01	9.3 ± 0.01
Kv4.3 [276FVPK]	6.8 ± 0.5	15.0 ± 0.1	16.5 ± 0.5	15.0 ± 0.5	−35.0 ± 0.04	5.6 ± 0.03	−31.5 ± 0.08	5.9 ± 0.07
K_V4.1 model	−1.5	19.6	14.8	22.6	N.A.	N.A.	N.A.	N.A.
K_V4.3 model	9.6	16.0	34.5	15.6	N.A.	N.A.	N.A.	N.A.

N.A., not applicable.

in determining the gating modification behavior of Kv4 channels in response to HpTx2. Therefore, we swapped amino acids 276 to 279 between Kv4.1 and Kv4.3 to give the mutant channels Kv4.1 [276VMTN] and Kv4.3 [276FVPK] and tested their response to the application of 2 μM HpTx2.

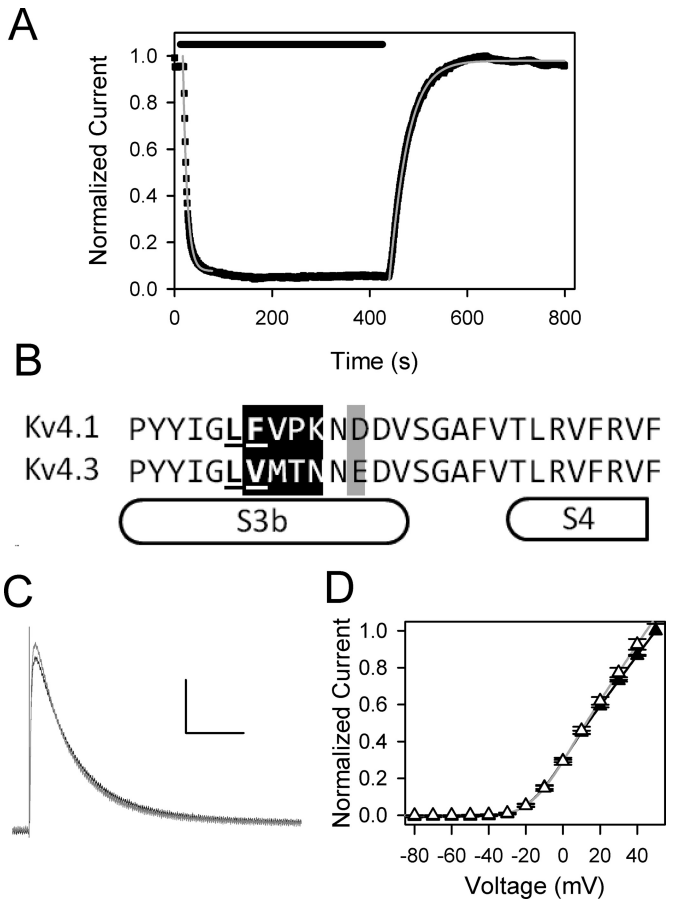

Fig. 2. The apparent HpTx2 binding site in the Kv4.3 S3b TMS is conserved in Kv4.1. A, determination of the apparent K_d value of HpTx2 for Kv4.1 as described previously (DeSimone et al., 2009). The pulse protocol and fitting algorithm are described under *Materials and Methods*. The horizontal bar shows the application time of 5 μM HpTx2. The squares represent the normalized tail current amplitude at −10 mV. Gray lines show the fits to the time courses of HpTx2 inhibition and washout. The best fits were derived assuming four independent binding sites: τ_{on} = 10.0 ± 1.3 s; τ_{off} = 28.2 ± 2.3 s (Table 2). B, alignment of the S3b TMS of Kv4.1 and Kv4.3. The boundaries of S3b and the aminoterminal portion of S4 are marked below (Long et al., 2007). The amino acids critical for HpTx2 gating modification (Leu275 and Val276) are shown in boldface type and are underlined. Nonconserved amino acids are shaded. C and D, HpTx2 does not modify gating of Kv4.1 [(L275,F276)A]. C, current traces of Kv4.1 [(L275,F276)A] in the presence of 5 μM HpTx2 (gray), performed and plotted as in Fig. 1C. D, the current-voltage relationship was determined as in Fig. 1. Closed triangles connected by a black line are the controls; open triangles connected by a gray line represent normalized current after application of 5 μM HpTx2. Data are shown as mean ± S.E.M., n = 6.

In the absence of toxin, the Kv4.3 and Kv4.1 mutants retain the basic current phenotype of their wild-type precursors (Fig. 3, A and E, compare with Fig. 1, C and D). Note that the $V_{1/2}$ and k values for G-V and SSIA are nearly identical between wild-type Kv4.1 and Kv4.1 [276VMTN] and likewise between wild-type Kv4.3 and Kv4.3 [276FVPK] (compare Fig. 1, A, B, and E–H, with Fig. 3, B–D and F–H; see Table 1). However, application of HpTx2 revealed dramatic differences between the wild-type and mutant phenotypes of the two channels. Kv4.1 [276VMTN] behaves toward 2 μM HpTx2 very similarly to wild-type Kv4.3 (Table 1). Like wild-type Kv4.3, the Kv4.1 S3b mutant has a high degree of voltage sensitivity toward toxin inhibition; 2 μM HpTx2 inhibits 39 and 82% of the Kv4.1 [276VMTN] current at 50 and 0 mV, respectively (Fig. 3B). The behavior of Kv4.1 [276VMTN] + 2 μM HpTx2 with respect to G-V is not identical with Kv4.3 but is still much more like Kv4.3 than Kv4.1 (Fig. 3E). The $\Delta V_{1/2}$ of the G-V for Kv4.1 [276VMTN] is 32.1 ± 2.4 mV compared with 22.0 ± 1.6 mV for Kv4.3 and 10.2 ± 1.2 mV for Kv4.1. Likewise, the shift in voltage-dependence of Kv4.1 [276VMTN] SSIA is nearly identical with that of Kv4.3; $\Delta V_{1/2}$ = 16.0 ± 0.02 for Kv4.1 [276VMTN] and 18.4 ± 2.1 for Kv4.3 (Fig. 3, C and I).

The reciprocal mutation, Kv4.3 [276FVPK], provides a mirror image of Kv4.1 [276VMTN]. In all respects, Kv4.3 [276FVPK] in the presence of HpTx2 behaves much more like wild-type Kv4.1 than Kv4.3. Kv4.3 [276FVPK] is 31% inhibited by 2 μM HpTx2 at +50 mV and 49% inhibited at 0 mV, close to the values of 36 and 54% obtained with wild-type Kv4.1 (Fig. 3F). Likewise the $\Delta V_{1/2}$ values for G-V and SSIA are all very close: 9.7 ± 0.7 mV and 3.5 ± 0.09 mV for Kv4.3 [276FVPK], compared with 10.2 ± 1.2 mV and 2.3 ± 0.06 mV for Kv4.1, respectively (Fig. 3, G and H; summarized in Fig. 3I and Table 1). This pattern also holds for the kinetics of gating modification and K_d (Fig. 3, J and K; Table 2), with the k_{on}, k_{off}, and K_d values of Kv4.3 [276FVPK] being close to those of Kv4.1, whereas the same parameters determined for Kv4.1 [276VMTN] are very close to those of wild-type Kv4.3. Taken together, these data show that four amino acids in S3b are capable of reversing the HpTx2 interaction phenotype of Kv4 channels between voltage-sensitive inhibition seen in Kv4.3 and the relatively voltage-insensitive interaction typical of Kv4.1.

Kinetic Modeling of HpTx2 Interaction with Kv4.1 and Kv4.3. The previous experiments allowed us to deduce the molecular basis of the differences in HpTx2-induced gating modification of Kv4.1 and Kv4.3. However, these data do not address the functional basis for these differences. Con-

TABLE 2
HpTx2 rate constants

Channel	τ_{on}	τ_{off}	k_{on}	k_{off}	K_d
	s		$M^{-1} \cdot s^{-1}$	s^{-1}	μM
K_V4.1*	10.0 ± 1.3	28.2 ± 2.3	5000 ± 650	0.0355 ± 0.0029	7.1 ± 1.1
K_V4.3	14.8 ± 2.0	51.8 ± 0.29	8450 ± 1140	0.0193 ± 0.00011	2.3 ± 0.3
K_V4.3 [276FVPK]	9.3 ± 1.6	22.4 ± 0.7	5380 ± 920[a]	0.0447 ± 0.0014	8.3 ± 1.5
K_V4.1 [276VMTN]	13.5 ± 2.0	61.7 ± 2.4	9260 ± 1370	0.0162 ± 0.00063	1.8 ± 0.3
K_V4.1 model	7.7	35	6490[a]	0.0286	4.4
K_V4.3 model	9.6	83.3	13020	0.0120	0.92

[a] k_{on} calculated in the presence of 5 μM HpTx2; unmarked rows calculated with 2 μM HpTx2. Kv4.3 rate constants are from DeSimone et al. (2009).

servation of the HpTx2 binding site in the two channels suggests that the answer does not lie in the mechanism of toxin interaction with the channel but in differences of its effect on activation and deactivation of Kv4.1 and Kv4.3.

To test this hypothesis, we took our previously described Markov model of Kv4.3 activation (Wang et al., 2004), and used experimentally derived data to develop a Markov model of Kv4.1 activation. The Markov model structure for activation in the absence of HpTx2 is described in scheme 1 (Fig. 4A). It includes four closed states (C_0–C_3), a preopen closed state (C_4), and an open state (O). Transitions between the closed states are voltage-dependent. The C_4 to O transition is voltage-independent. Kv4.1 and Kv4.3 have four subunits, and the model assumes that each subunit must be activated before the channel can conduct ions. The model parameters are described in Table 3.

We obtained the rate constants for Kv4.3 and Kv4.1 model development based on experimental results from the voltage dependence of activation, deactivation, and G/G_{max}. These experiments were performed at 16°C to slow the activation and deactivation rates, which kept signals from being obscured by the capacitance transient, allowing accurate assessment of τ_{act} and τ_{deact} (Fig. 5, A and B). The model simulates the voltage-dependence of τ_{act} and τ_{deact} that are well fit to the experimental data (Fig. 5, C–F). The forward rate constants (α) and voltage-independent rate constants (k_{co} and k_{oc}) are the same in both models. Deactivation is slower in Kv4.1 than in Kv4.3 ($\tau_{deact,\ Kv4.1} = 7.2 \pm 0.3\ ms^{-1}$, and $4.8 \pm 0.3\ ms^{-1}$ for Kv4.3, both at −120 mV; Fig. 5, E and F); to account for this, we reduced the reverse rate constant (β) by a factor of 0.82 in Kv4.1 (Table 3).

Because the toxin binding experiments were conducted at room temperature (approximately 21°C), the derived values of the forward (α) and reverse (β) rate constants at 16°C were multiplied by the square root of the Q_{10} (3.17 ± 0.54) (Campbell et al., 1993) to compensate for temperature differences. This compensation gives similar results obtained during the development of our original Kv4.3 model (Wang et al., 2004), suggesting that it is valid for Kv4.1 activation as well. To model the effect of HpTx2 on Kv4.1 and Kv4.3, we assumed that one toxin molecule could bind to each subunit and that each subunit activates independently. This results in independent modification of the transition rates for activation-deactivation of toxin-bound subunits. Combining the activation model of scheme 1 (Fig. 4A) with a kinetic model for toxin binding (Swartz and MacKinnon, 1997), we constructed a 30-state Markov model for toxin-channel interaction illustrated in scheme 2 (Fig. 4B). In this model, each closed state

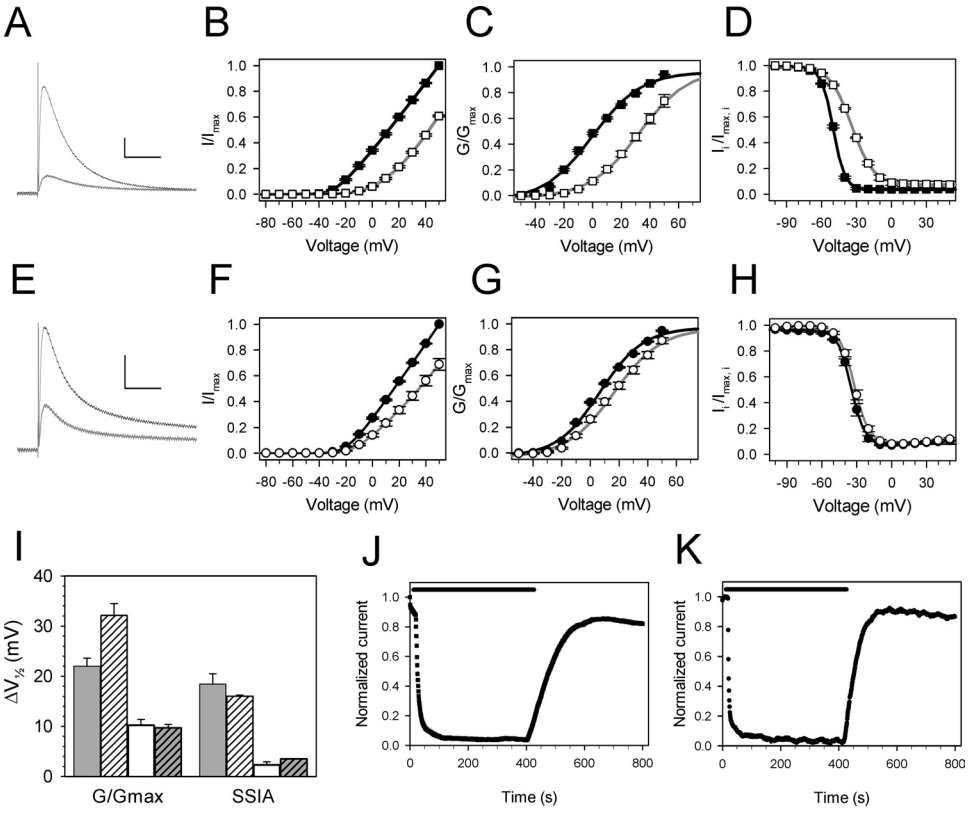

Fig. 3. The S3b "swap" mutants exchange phenotypes between Kv4.3 and Kv4.1 with regard to HpTx2 interaction. Top are from Kv4.1[VMTN] (square symbols; A–D), and the middle row are from Kv4.3[FVPK] (circles; E and F). A and E, representative current traces of Kv4.1[VMTN] and Kv4.3[FVPK], respectively, in the presence of 2 μM HpTx2 (gray), performed and plotted as in Fig. 1C. B to D, normalized I-V, G-V, and voltage-dependence of steady-state inactivation of Kv4.1 [275VMTN] in response to application of HpTx2. G and H, normalized I-V, G-V, and voltage-dependence of steady-state inactivation of Kv4.3 [275FVPK] in response to application of HpTx2. I, summary of the shifts in voltage-dependence of conductance and steady-state inactivation (expressed as $\Delta V_{1/2}$, summarized in Table 1) of the wild-type and mutant channels in response to toxin. The shaded bars represent Kv4.3, the open bars Kv4.1; the shaded crosshatched bars represent Kv4.3 [275FVPK], and the open crosshatched bars are Kv4.1 [275VMTN]. The control values for each of the S3b swap mutant channels are nearly identical with those of its wild-type parent. J and K, changing the S3b sequence swaps HpTx2 inhibition time courses. Representative experiments showing Kv4.1 [275VMTN] (J) in the presence of 2 μM HpTx2, and Kv4.3 [275FVPK] with 5 μM HpTx2 (K). The time courses were fit as in Fig. 2A, assuming four toxin binding sites. The time constants and K_d values are listed in Table 2. The pulse protocols and fitting algorithms are described in *Materials and Methods.* B to D and F to I are presented as mean values ± S.E.M, $n = 6$.

can be occupied by up to four toxin molecules. At −90 mV, HpTx2 binds to the closed state of Kv4 channels; these closed states have four "nonactivated" subunits through the toxin binding pathway from C_0 to CB_{04} (see Fig. 2A and DeSimone et al. (2009); transitions C_0 to CB_{04} in Fig. 4B with rates k_{on} and k_{off}). This gives the models five subpopulations of channels whose activation pathways can accommodate up to four bound toxin molecules. Activation and deactivation kinetics of the channels are roughly 3 orders of magnitude faster than toxin on and off rates, strongly suggesting that the channels will retain bound toxin in the open state. This is shown in the model as one unbound open state O, and four open states with bound toxin (OB_1–OB_4; Fig. 4B).

To determine transition rates between states in the Markov model, we used experimental data of the influence of HpTx2 on Kv4.3 and Kv4.1 I-V and G-V relationships and activation and deactivation kinetics. The models postulate that binding of one toxin molecule changes the activation and deactivation rate constants for each channel subunit. For example, when one toxin molecule is bound to the channel, the total transition rate from CB_{01} to CB_{11}, is $\alpha_T + 3\alpha$ (Fig. 4B). There are 12 possible transitions from CB_{11} to CB_{21} (two activated subunits): 3 with a rate of α_T, and 9 with rates equal to α, yielding a net transition rate of $\frac{3}{4}(\alpha_T + 3\alpha)$. Likewise, deactivation rate constants from CB_{21} to CB_{11} to CB_{01} are $\beta_T + 3\beta$ and $1/4(\beta_T + 3\beta)$, respectively. Identical reasoning was used to assign the voltage-dependent rate constants to the remainder of the transitions in scheme 2.

The rules are similar for voltage-independent transitions. The modified transition rates for each subunit (k_{coT} and k_{ocT}), result in the voltage-independent rates $1/4[ik_{coT} + (4 - i)k_{co}]$ and $1/4[ik_{ocT} + (4 - i)k_{oc}]$, where i is the number of toxin molecules bound to the channel. The association and dissociation rates between toxin-bound states with at least one activated subunit were modified to fulfill the conditions of detailed thermodynamic equilibrium. For example, for transitions between CB_{11} and CB_{12}, coefficients $t_{\alpha 2}$ and $t_{\beta 2}$ are defined as

$$t_{\alpha 2} = \frac{2\alpha_T + 2\alpha}{\alpha_T + 3\alpha} \text{ and } t_{\beta} = \frac{2\beta_T + 2\beta}{\beta_T + 3\beta}$$

which result in equal clockwise and counter-clockwise products of rate constants between states CB_{01}, CB_{11}, CB_{12}, and CB_{02}. Likewise, from detailed thermodynamic equilibrium we can define coefficients t_{coT2} and t_{ocT2} as

$$t_{coT2} = t_{\alpha 2}^4 \frac{2k_{coT} + 2k_{co}}{k_{coT} + 3k_{co}} \text{ and } t_{ocT2} = t_{\alpha 2}^4 \frac{2k_{ocT} + 2k_{oc}}{k_{ocT} + 3k_{oc}}$$

for the transitions between CB_{41}, OB_1, OB_2, and CB_{42}. All rate other constants for the 30-state Markov model can be found in Fig. 4B.

The rate constants that were changed to account for HpTx2 interaction with Kv4.1 and Kv4.3 are summarized in Table 3. Application of 2 μM HpTx2 increased the time-to-peak current by 10 and 20% at for Kv4.1 and Kv4.3, respectively (Fig. 5, G and H), making the activation rate constants $\alpha_T = 0.9\alpha$ for Kv4.1 and $\alpha_T = 0.8\alpha$ for Kv4.3. Deactivation of both channels accelerated by a factor of 2, so that $\beta_T = 2\beta$ for both Kv4.1 and Kv4.3. To account for the differences in the toxin effect on current-voltage and conductance-voltage relationships (Fig. 1, A–F), the values of k_{coT} were reduced to 5400 and 4000 s^{-1} for Kv4.1 and Kv4.3, respectively, from 6000 s^{-1} without toxin. Likewise, k_{ocT} was increased from 1500 s^{-1} without toxin to 9000 and 3000 s^{-1}.

The Markov model of Kv4.3 and Kv4.1 activation incorporating HpTx2-bound states produces simulated data that gives the optimized fits to the experimental data. The model predicts that the k_{on} at 5 μM HpTx2 for Kv4.1 is 6490 $M^{-1} \cdot s^{-1}$ and a k_{off} of 0.0286 s^{-1} compared with the experimentally

A

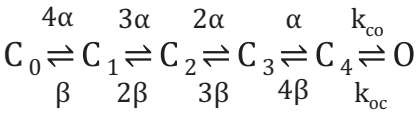

Scheme 1

B

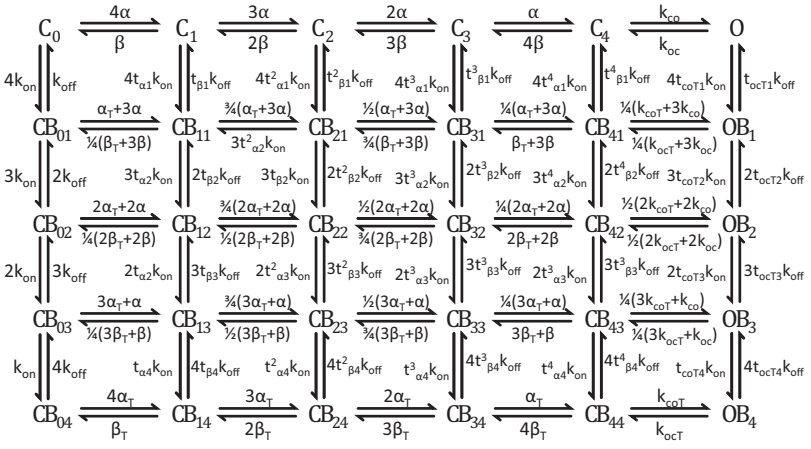

Scheme 2

Fig. 4. Modeling schemes. A, scheme 1 is a Markov model for Kv4.3 or Kv4.1 in the absence of toxin. B, scheme 2 shows the addition of four toxin-bound states for each state in scheme 1. The parameters used to generate the model are in Table 3.

determined 5000 ± 650 $M^{-1} \cdot s^{-1}$ and 0.0355 ± 0.0029 s^{-1}, respectively, giving a predicted K_d of 4.4 μM compared with the experimentally determined 7.1 ± 1.1 μM. Likewise, the predicted k_{on}, k_{off}, and K_d of 2 μM HpTx2 for Kv4.3 were 13,020 $M^{-1} \cdot s^{-1}$, 0.0120 s^{-1}, and 0.92 μM compared with the experimentally determined values of 8450 ± 1140 $M^{-1} \cdot s^{-1}$, 0.0193 ± 0.00011 s^{-1}, and 2.3 ± 0.3 μM, respectively (Fig. 6A, and Table 1). In both cases, the predicted K_d is approximately 2-fold lower; however, the affinity constants maintain their relative values with respect to the two channels.

In developing the model, we made minimal changes to the specified parameters based on the experimental data. Changing other gating parameters did not produce a model that fit experimental data. Specifically, changes in rate constants (α and β) of the voltage-dependent steps of the Kv4.1 activation model created shifts in the normalized G-V relationship that did not fit the experimental data; the changes in k_{OC} were the only variation we found that mimicked the effects of HpTx2.

Likewise, the simulated data of the toxin's influence on the current and conductance-voltage relationships reproduced the experimental data well. The outstanding difference in HpTx2-induced I-V relationships between Kv4.3 and Kv4.1 was the degree of voltage-dependent inhibition. The model predicts that 2 μM HpTx2 will inhibit 53% of Kv4.1 K^+ current at 0 mV and only 31% at 50 mV compared with the experimental data of 54 ± 5 and 36 ± 2%, respectively (Fig. 6B). For Kv4.3 inhibition at 0 mV, the model predicts 81% compared with the measured value of 80 ± 3% and at 50 mV, 45% compared with the measured value of 37 ± 3% (Fig. 6C). The $\Delta V_{1/2}$ in G/G_{max} for Kv4.1 upon application of 2 μM HpTx2 was 10.2 ± 1.2 mV, close to the 16.3 mV predicted by the model. Under the same conditions, Kv4.3 shifts 22.0 ± 1.6 mV, approximately 3 mV less than the predicted 24.9 mV shift (Fig. 6, D and E). These close approximations suggest that the observed differences in Kv4.1 and Kv4.3 gating upon HpTx2 application are due to differences in modification of the kinetics of both the voltage-dependent and voltage-independent transitions occurring during channel activation and deactivation.

TABLE 3
Model parameters

Calculation of rate constants of activation in 2 mM K^+: $\alpha = f\alpha\ (a_1 \exp(z_{\alpha 1}\ VF/RT)\ \exp((V + 10.0)/10.0) + a_2 \exp(z_{\alpha 2}\ VF/RT))$; $\beta = f\beta\ (b_1 \exp(z_{\beta 1}\ VF/RT)\ \exp((V + 5.0)/10.0) + b_2 \exp(z_{\beta 2}\ VF/RT))$, where factors $f\alpha = 1/(1 + \exp((V + 10.0)/10.0))$ and $f\beta = 1/(1 + \exp((V + 5.0)/10.0))$, where V is voltage, F is the Faraday constant, R is the gas constant, and T is absolute temperature. Net current through the channel is given by $I = G_{max}P_O(V - E_K)$, where $E_K = (RT/F)ln([K^+]_o/[K^+]_i)$.

Parameter	Control		+2 μM HpTx2	
	Kv4.1	Kv4.3[a]	Kv4.1	Kv4.3
a_1 (s^{-1})	276.25	276.25	248.63	221.00
$z_{\alpha 1}$	0.27	0.27	0.27	0.27
a_2 (s^{-1})	54.34	54.34	48.91	43.47
$z_{\alpha 2}$	0.83	0.83	0.83	0.83
b_1 (s^{-1})	201.96	246.84	201.96	493.68
$z_{\beta 1}$	−0.54	−0.54	−0.54	−0.54
b_2 (s^{-1})	22.68	27.72	22.68	55.44
$z_{\beta 2}$	−0.48	−0.48	−0.48	−0.48
k_{co} (s^{-1})	6000	6000	5400	4800
k_{oc} (s^{-1})	1500	1500	9000	3000
k_{on} ($M^{-1} \cdot s^{-1}$)			6490	13,020
k_{off} (s^{-1})			0.0286	0.012

[a] From Wang et al. (2004).

Discussion

Heteropoda toxin 2 is one of many ICK toxins that are voltage-dependent gating modifiers of mammalian voltage-gated K^+ channels (Swartz, 2007). However, HpTx2 is the first K^+ gating modifier toxin to show the type of isoform-specific voltage-dependent properties demonstrated by our data. To understand this novel observation, we identified the molecular basis of the differences in gating modification of Kv4.3 and Kv4.1 by HpTx2. We then developed a 30-state Markov model that can account for how the toxin influences the two channels differently. To our knowledge, this is the first detailed study to examine the mechanism of these dif-

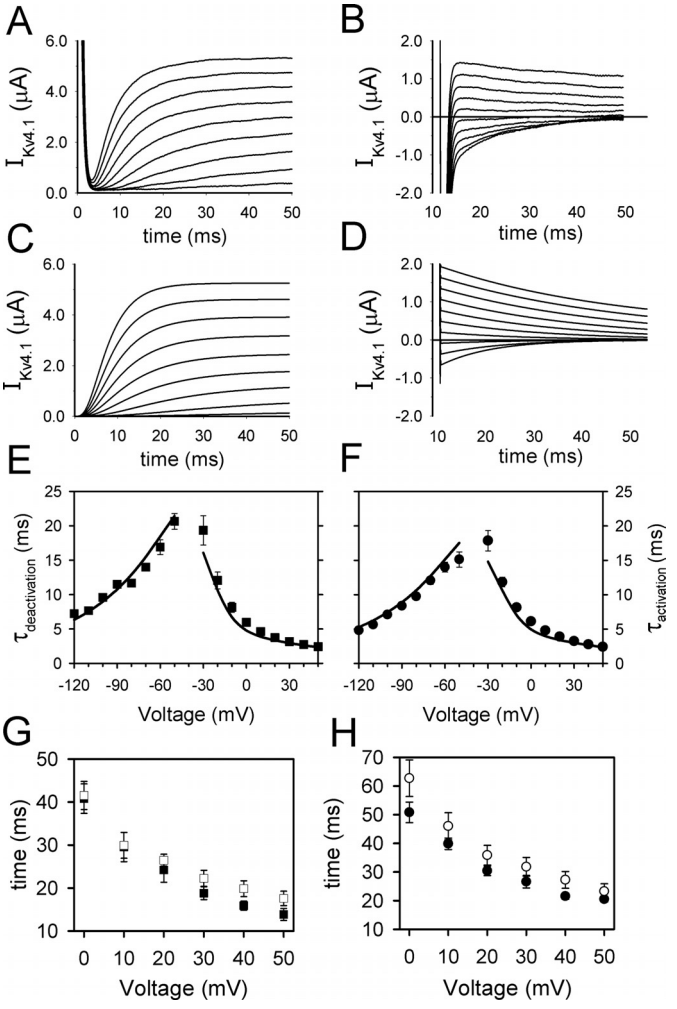

Fig. 5. The Kv4 activation model reproduces both Kv4.1 activation and deactivation. A, current traces of activation versus time after pulses to −30 to +50 mV in 10-mV increments from the −90 mV holding potential. B, current traces of deactivation from a +50-mV pulse to a range of voltages from −120 to −50 mV in 10-mV increments. C and D, simulations of the experiments in A and B. E and F, activation and deactivation time constants for Kv4.1 (E) and Kv4.3 (F) plotted against voltage. The solid lines represent predictions derived from the Kv4 activation models. The experimental data were collected at 16°C, and the simulations were performed with the model parameters adjusted to 16°C (reduction of the rate constants by a factor 1.78 and replacement of T = 295 K by T = 289 K). G and H, time to peak current for Kv4.1 and Kv4.3 in the presence of HpTx2. Protocol is the same as in Fig. 1A, from a holding potential of −90 mV for Kv4.1 (A; squares) and Kv4.3 (B; circles) in the presence of 2 μM HpTx2 (open symbols). The pulse protocols and fitting functions are described under *Materials and Methods*. Data are plotted as mean ± S.E.M., n = 4–6.

ferences and to apply this knowledge to enhance our understanding of Kv4 channel gating.

The model accounts for the difference in voltage-dependent inhibition between Kv4.1 and Kv4.3 by HpTx2. Experimental data showed approximately a 3-fold difference in apparent K_d for HpTx2 binding to the two channels (Table 2). The larger Kv4.1 K_d results in a smaller number of toxin-bound channels in the C_{01} to C_{34} states at any given voltage; therefore, more channels follow the direct activation pathway from C_0 to O. The result is the comparatively small depolarizing shift in Kv4.1 G-V relationship in the presence of toxin. However, Kv4.1 and Kv4.3 are inhibited by toxin to nearly the same degree at +50 mV. To account for this, we increased the toxin-bound voltage-independent rate (k_{oc}) 2-fold in the Kv4.3 model and 6-fold in the Kv4.1 model, resulting in a more stable Kv4.1 C_4 state. The higher affinity of HpTx2 for Kv4.3 results in greater inhibition during the voltage-dependent steps. Therefore, a smaller decrease in k_{co} gives the same degree of inhibition of Kv4.3 by HpTx2.

The probabilities of finding Kv4.1 and Kv4.3 in the presence of toxin in closed and open states (state occupancies) are illustrated in Fig. 7. At −50 mV, lower than the threshold for

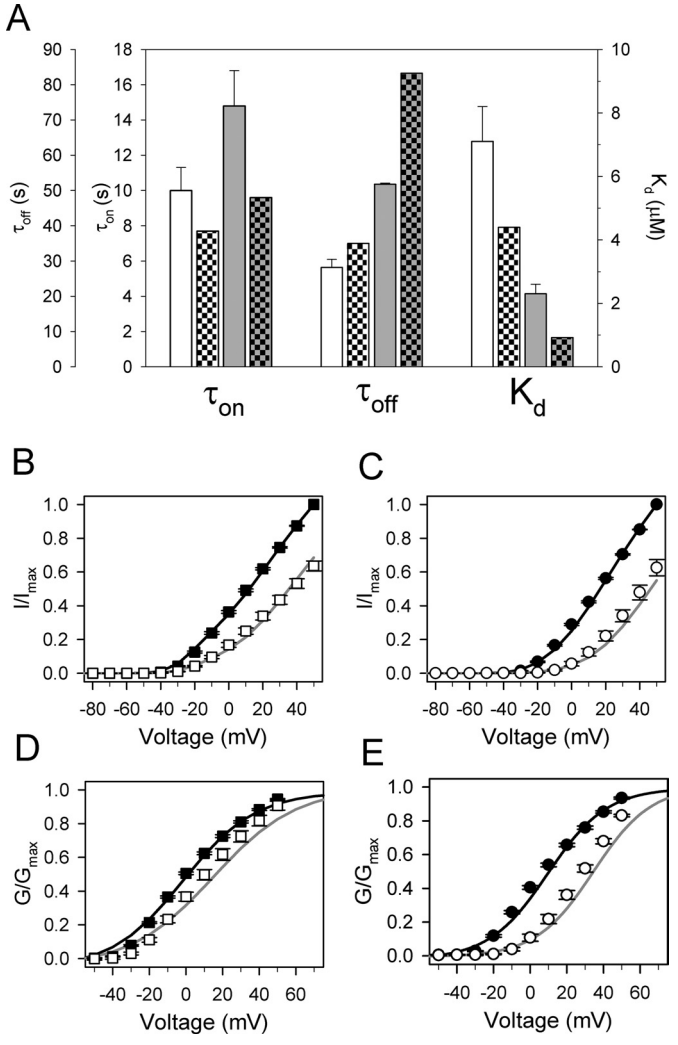

Fig. 6. The Kv4 activation models reproduce HpTx2 gating modification. A, time courses of interaction (represented as τ_{on} and τ_{off}), and dissociation constants for Kv4.1 (white) and Kv4.3 (gray). Open bars represent experimental data as mean ± S.E.M., $n = 6$, calculated from Fig. 2A for Kv4.1 or from DeSimone et al. (2009) for Kv4.3. Values predicted by our Markov model are shown in adjacent bars (checkered). B to E, actual and predicted normalized I-V (B and C) and G-V relationships (D and E) for Kv4.1 (B and D) and Kv4.3 (C and E) under control conditions (filled symbols) or in the presence of 2 μM HpTx2 (open symbols). The data are from Fig. 1, A and B, whereas the line is that predicted by our Markov model; black lines are under control conditions, and gray lines represent the presence of toxin.

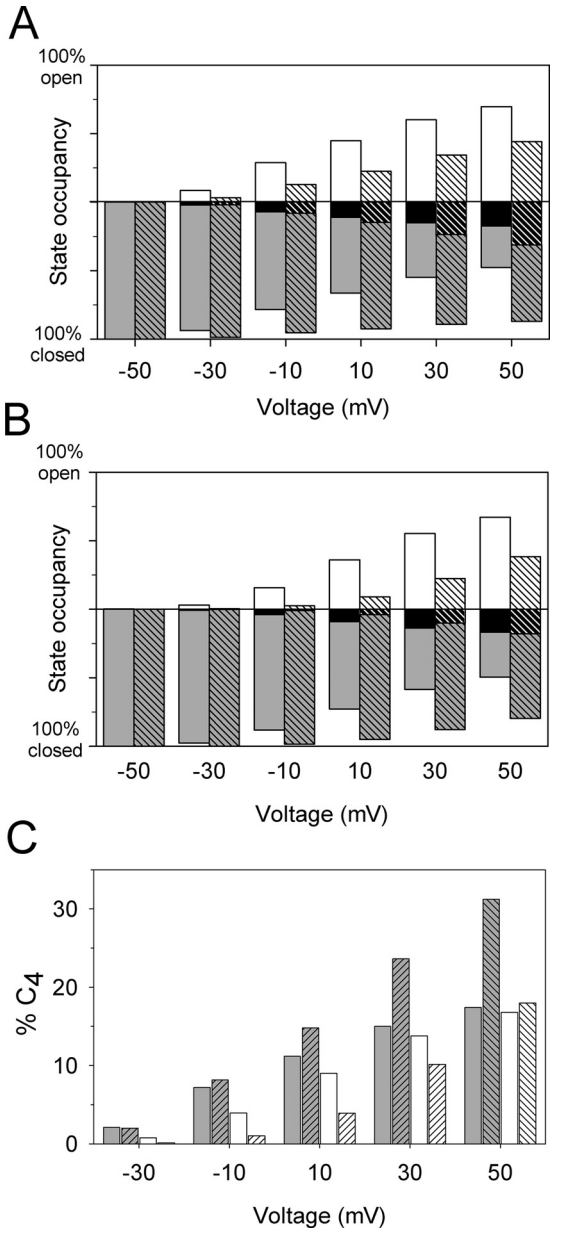

Fig. 7. The voltage-dependencies of state occupancy explain the differences in HpTx2 voltage-dependence in Kv4.3 and Kv4.1. A and B, relative state occupancy of Kv4.1 (A) and Kv4.3 (B) at different voltages in the absence (open bars) and presence of 2 μM HpTx2 (cross-hatched bars). Positive values represent the proportion of channels that are open (in white). Values below the origin represent channels occupying a closed state: C_0 to C_3 are gray, and C_4 is black. A bar completely below the origin represents channels that occupy only closed states, whereas a bar completely above the origin represents channels that are 100% open. In the presence of toxin and at low voltages, more toxin bound Kv4.1 channels open than toxin bound Kv4.3 channels because of the lower voltage-dependence of the Kv4.1 C_0 to C_3 transitions, but as voltages increase, accumulation of toxin bound Kv4.1 in the C_4 state is more prominent. C, the influence of 2 μM HpTx2 (crosshatched bars) on the relative occupancy of Kv4.1 (gray) and Kv4.3 (white) in the C_4 state. The increasing prominence of the C_4 state in toxin-bound Kv4.1 correlates with the lack of voltage sensitivity of the HpTx2-Kv4.1 interaction.

activation, both channels are in the C_0 to C_3 states regardless of HpTx2 presence. As the voltage increases to −10 mV in the absence of toxin, a significant fraction of channels open: 29% of Kv4.1 (Fig. 7A) and 16% of Kv4.3 (Fig. 7B); only 7% of Kv4.1 and 4% of Kv4.3 occupy the C_4 state (Fig. 7C). With the addition of 2 μM HpTx2, a negligible number of Kv4.3 channels are in the open and C_4 states at −10 mV. However, a significant fraction of Kv4.1 channels are open (13%) and in the C_4 (8%) states under these conditions, which is reflected the lower degree of voltage-dependence of HpTx2 interaction with Kv4.1. At +30 mV in the absence of HpTx2, the two channels have approximately the same proportion of open, C_0 to C_3, and C_4 states. In the presence of toxin, the number of open state channels is decreased in favor of closed states for both channels; however, the fraction of Kv4.1 in C_4 state is 24% compared with only 10% of Kv4.3. The relatively large effect of HpTx2 on the voltage-independent transition from C_4 to O of Kv4.1 results in higher occupation of the C_4 state, thus accounting for the low degree of voltage dependence of HpTx2 modification of Kv4.1 gating.

In developing models to account for the effects of HpTx2 on Kv4.3 and Kv4.1, we restricted ourselves to a description of the toxin's effects on Kv4.3 and Kv4.1 activation. Eliminating inactivation from our models of HpTx2 gating modification is possible because all forms of inactivation in Kv4.1 and Kv4.3 are much slower than activation and deactivation in the presence of HpTx2. These rate differences allow measurement of activation and deactivation at time scales that do not allow significant development of inactivation.

Eliminating inactivation also greatly simplified model development but still allowed us to account for our experimental observations. This is not surprising; aside from the long time constants involved in inactivation, our previous studies showed that HpTx2 has very modest effects on Kv4 inactivation kinetics (Zarayskiy et al., 2005). Furthermore, the shifts in $V_{1/2}$ steady-state inactivation induced by HpTx2 (Fig. 1, G and H) mirror the shifts in $V_{1/2}$ calculated from the G-V relationship, the result being a much smaller $\Delta V_{1/2}$ for Kv4.1 than for Kv4.3 ($\Delta V_{1/2,SSIA}$ = 2.3 ± 0.06 mV for Kv4.1 and 18.4 ± 2.1 mV for Kv4.3; Table 1). This behavior probably reflects the coupling of Kv4 inactivation to activation. Although a full consideration of inactivation in our Markov models might have contributed some insight to Kv4 inactivation, our goal was to understand the differences in behavior observed between Kv4.3 and Kv4.1 in the presence of HpTx2. The success of our model in recapitulating our experimental data argues that the assumptions behind its development (i.e., not including inactivation) are valid and that inactivation is not important to understanding our observations.

Our previous work has shown that the critical amino acids for HpTx2 gating modification of Kv4.3 are a leucine and valine dyad at amino acid 275 in transmembrane segment S3b (DeSimone et al., 2009). In Kv4.1, the required amino acids are a conserved leucine and a phenylalanine at the homologous position in S3b (Fig. 2B). In addition to the binding sites being similar, we have also shown that the number of potential binding sites between the two channels is identical. However, the most striking feature of HpTx2 interaction with Kv4.3 and Kv4.1 is the difference in the degree of voltage sensitive inhibition. We have established that this effect is solely due to four nonidentical amino acids in S3b that overlap with the HpTx2 binding site. Individual point mutations of the four nonconserved amino acids had little effect on voltage dependence, except for P278T (in Kv4.1; data not shown), whose effects were similar but not as dramatic as those of Kv4.3[276FVPK] and Kv4.1[276VMTN], which effectively reversed the gating modification phenotype (Fig. 3). The existence of proline 278 in Kv4.1 is unique; there are no other occurrences at the homologous position in any known voltage-gated K^+ channel. The S3b of Kv2.1 forms an α helix through this position (Long et al., 2007); however, proline is well known for its inability to fit into internal positions in helices and is most often associated with turns (Richardson and Richardson, 1989), suggesting that the structure of *Shal* channel S3b may not be well conserved with Kv2.1.

Gating modifier toxins similar to HpTx2 interact with the outward facing portion of the VSD, sitting between the VSD and the pore domain, in which they are well positioned to interfere with the translational and rotational movement of the VSDs that lead to opening of the channel pore (Milescu et al., 2009; Wee et al., 2010). The VSD has been implicated in the transition from the voltage-independent preopen closed state (C_4) to the open state (Schoppa and Sigworth, 1998; Zandany et al., 2008). We show that much of the inhibition of Kv4.1 by HpTx2 must be occurring during this final, voltage-independent step, suggesting an important role for S3b movement in the transition. On the other hand, the different S3b sequence of Kv4.1 might allow HpTx2 to interfere with the concerted conformational changes in each pore domain subunit required for channel opening. Although we lack the structural data required to distinguish these hypotheses, we believe that this study emphasizes the unique value of gating modifier toxins in understanding activation kinetics and their relation to voltage-sensor structure and movement in voltage-gated ion channels.

HpTx2 is 1 of 18 peptide toxins reported to interact with a member of the Kv4 family (Herzig et al., 2011), all of which share the inhibitor cysteine knot tertiary structure and were purified from spider venom. Of these, three others have been shown to discriminate between Kv4.3 (or Kv4.2) and Kv4.1 but not to interact with other voltage-gated channels. Two were purified from the *Phrixotrichus auratus* venom, PaTx1 and PaTx2, with PaTx1 being the more potent of the two (Diochot et al., 1999); these toxins share approximately 50% sequence identity with HpTx2. PaTx1 inhibition of Kv4.3 is similar to that of HpTx2 except that it significantly slows inactivation kinetics and recovery from inactivation. It is also a weaker inhibitor of Kv4.1 currents. In contrast, A toxin 79% identical with PaTx1, JZTX-XII purified from *Chilobrachys jingzhao* venom, is a relatively strong inhibitor of Kv4.1 and a much weaker inhibitor of Kv4.2 (Yuan et al., 2007); HpTx2 inhibits Kv4.2 to roughly the same degree as Kv4.3 (Zarayskiy et al., 2005). Although it is likely these three toxins interact with Kv4 channels at or near the S3b HpTx2 binding site, this assumption has not been tested experimentally. We have shown differences previously in the affinity of HpTx2 for Kv4.3 associated with an ancillary subunit (DeSimone et al., 2009); in this work, we have shown how to distinguish Kv4.1 currents from Kv4.3 (and probably Kv4.2) currents using this toxin. Although we have not tested all combinations of Kv4 channel and ancillary subunit for their current phenotype in response to HpTx2, we believe that this toxin, perhaps in combination with other Kv4-specific peptide toxins, will prove to be useful in unambiguous

identification of the molecular basis of transient outward K^+ currents.

Acknowledgments

We thank Dr. Chang Xie for preparation of oocytes, YiChun Lu for preparation of RNA, Dr. Larry Salkoff for the gift of the Kv4.1 construct, and Dr. Randall Rasmusson for advice, support, and encouragement.

Authorship Contributions

Participated in research design: DeSimone, Bondarenko, and Morales.

Conducted experiments: DeSimone and Zarayskiy.

Contributed new reagents or analytic tools: Bondarenko and Morales.

Performed data analysis: DeSimone, Zarayskiy, Bondarenko, and Morales.

Wrote or contributed to the writing of the manuscript: DeSimone, Bondarenko, and Morales.

References

Bähring R and Covarrubias M (2011) Mechanisms of closed-state inactivation in voltage-gated ion channels. *J Physiol* **589:**461–479.

Birnbaum SG, Varga AW, Yuan LL, Anderson AE, Sweatt JD, and Schrader LA (2004) Structure and function of Kv4-family transient potassium channels. *Physiol Rev* **84:**803–833.

Brahmajothi MV, Campbell DL, Rasmusson RL, Morales MJ, Trimmer JS, Nerbonne JM, and Strauss HC (1999) Distinct transient outward potassium current (I_{to}) phenotypes and distribution of fast-inactivating potassium channel alpha subunits in ferret left ventricular myocytes. *J Gen Physiol* **113:**581–600.

Campbell DL, Rasmusson RL, Qu Y, and Strauss HC (1993) The calcium-independent transient outward potassium current in isolated ferret right ventricular myocytes. I. Basic characterization and kinetic analysis. *J Gen Physiol* **101:** 571–601.

Catterall WA, Cestèle S, Yarov-Yarovoy V, Yu FH, Konoki K, and Scheuer T (2007) Voltage-gated ion channels and gating modifier toxins. *Toxicon* **49:**124–141.

Covarrubias M, Bhattacharji A, De Santiago-Castillo JA, Dougherty K, Kaulin YA, Na-Phuket TR, and Wang G (2008) The neuronal Kv4 channel complex. *Neurochem Res* **33:**1558–1567.

DeSimone CV, Lu Y, Bondarenko VE, and Morales MJ (2009) S3b amino acid substitutions and ancillary subunits alter the affinity of Heteropoda venatoria toxin 2 for Kv4.3. *Mol Pharmacol* **76:**125–133.

Diochot S, Drici MD, Moinier D, Fink M, and Lazdunski M (1999) Effects of phrixotoxins on the Kv4 family of potassium channels and implications for the role of I_{to1} in cardiac electrogenesis. *Br J Pharmacol* **126:**251–263.

Dutertre S and Lewis RJ (2010) Use of venom peptides to probe ion channel structure and function. *J Biol Chem* **285:**13315–13320.

Estrada G, Villegas E, and Corzo G (2007) Spider venoms: a rich source of acylpolyamines and peptides as new leads for CNS drugs. *Nat Prod Rep* **24:**145–161.

Gracy J, Le-Nguyen D, Gelly JC, Kaas Q, Heitz A, and Chiche L (2008) KNOTTIN: the knottin or inhibitor cystine knot scaffold in 2007. *Nucleic Acids Res* **36:**D314–D319.

Herzig V, Wood DL, Newell F, Chaumeil PA, Kaas Q, Binford GJ, Nicholson GM, Gorse D, and King GF (2011) ArachnoServer 2.0, an updated online resource for spider toxin sequences and structures. *Nucleic Acids Res* **39:**D653–D657.

Himmel HM, Wettwer E, Li Q, and Ravens U (1999) Four different components contribute to outward current in rat ventricular myocytes. *Am J Physiol* **277:** H107–H118.

Hodgson WC and Isbister GK (2009) The application of toxins and venoms to cardiovascular drug discovery. *Curr Opin Pharmacol* **9:**173–176.

Institute of Laboratory Animal Resources (1996) *Guide for the Care and Use of Laboratory Animals* 7th ed. Institute of Laboratory Animal Resources, Commission on Life Sciences, National Research Council, Washington DC.

Kassiri Z, Zobel C, Nguyen TT, Molkentin JD, and Backx PH (2002) Reduction of I_{to} causes hypertrophy in neonatal rat ventricular myocytes. *Circ Res* **90:**578–585.

Lewis RJ and Garcia ML (2003) Therapeutic potential of venom peptides. *Nat Rev Drug Discov* **2:**790–802.

Liu J, Kim KH, London B, Morales MJ, and Backx PH (2011) Dissection of the voltage-activated potassium outward currents in adult mouse ventricular myocytes: $I_{to,f}$, $I_{to,s}$, $I_{K,slow1}$, $I_{K,slow2}$, and I_{ss}. *Basic Res Cardiol* **106:**189–204.

Long SB, Tao X, Campbell EB, and MacKinnon R (2007) Atomic structure of a voltage-dependent K^+ channel in a lipid membrane-like environment. *Nature* **450:**376–382.

Milescu M, Bosmans F, Lee S, Alabi AA, Kim JI, and Swartz KJ (2009) Interactions between lipids and voltage sensor paddles detected with tarantula toxins. *Nat Struct Mol Biol* **16:**1080–1085.

Nerbonne JM, Gerber BR, Norris A, and Burkhalter A (2008) Electrical remodelling maintains firing properties in cortical pyramidal neurons lacking KCND2-encoded A-type K^+ currents. *J Physiol* **586:**1565–1579.

Nerbonne JM and Kass RS (2005) Molecular physiology of cardiac repolarization. *Physiol Rev* **85:**1205–1253.

Ramakers GM and Storm JF (2002) A postsynaptic transient K^+ current modulated by arachidonic acid regulates synaptic integration and threshold for LTP induction in hippocampal pyramidal cells. *Proc Natl Acad Sci USA* **99:**10144–10149.

Richardson JS and Richardson DC (1989) Principles and Patterns of Protein Conformation, in *Prediction of Protein Structure and the Principles of Protein Conformation* (Fasman GD ed) pp 2–98, Plenum Press, New York.

Sanguinetti MC, Johnson JH, Hammerland LG, Kelbaugh PR, Volkmann RA, Saccomano NA, and Mueller AL (1997) Heteropodatoxins: peptides isolated from spider venom that block Kv4.2 potassium channels. *Mol Pharmacol* **51:**491–498.

Schoppa NE and Sigworth FJ (1998) Activation of *Shaker* potassium channels. II. Kinetics of the V2 mutant channel. *J Gen Physiol* **111:**295–311.

Swartz KJ (2007) Tarantula toxins interacting with voltage sensors in potassium channels. *Toxicon* **49:**213–230.

Swartz KJ and MacKinnon R (1995) An inhibitor of the Kv2.1 potassium channel isolated from the venom of a Chilean tarantula. *Neuron* **15:**941–949.

Swartz KJ and MacKinnon R (1997) Hanatoxin modifies the gating of a voltage-dependent K^+ channel through multiple binding sites. *Neuron* **18:**665–673.

Varga AW, Yuan LL, Anderson AE, Schrader LA, Wu GY, Gatchel JR, Johnston D, and Sweatt JD (2004) Calcium-calmodulin-dependent kinase II modulates Kv4.2 channel expression and upregulates neuronal A-type potassium currents. *J Neurosci* **24:**3643–3654.

Wang S, Bondarenko VE, Qu YJ, Bett GC, Morales MJ, Rasmusson RL, and Strauss HC (2005) Time- and voltage-dependent components of Kv4.3 inactivation. *Biophys J* **89:**3026–3041.

Wang S, Bondarenko VE, Qu Y, Morales MJ, Rasmusson RL, and Strauss HC (2004) Activation properties of Kv4.3 channels: time, voltage and $[K^+]_o$ dependence. *J Physiol* **557:**705–717.

Wang S, Patel SP, Qu Y, Hua P, Strauss HC, and Morales MJ (2002) Kinetic properties of Kv4.3 and their modulation by KChIP2b. *Biochem Biophys Res Commun* **295:**223–229.

Wee CL, Gavaghan D, and Sansom MS (2010) Interactions between a voltage sensor and a toxin via multiscale simulations. *Biophys J* **98:**1558–1565.

Yuan C, Liao Z, Zeng X, Dai L, Kuang F, and Liang S (2007) Jingzhaotoxin-XII, a gating modifier specific for Kv4.1 channels. *Toxicon* **50:**646–652.

Zandany N, Ovadia M, Orr I, and Yifrach O (2008) Direct analysis of cooperativity in multisubunit allosteric proteins. *Proc Natl Acad Sci USA* **105:**11697–11702.

Zarayskiy VV, Balasubramanian G, Bondarenko VE, and Morales MJ (2005) *Heteropoda* toxin 2 is a gating modifier toxin specific for voltage-gated K^+ channels of the Kv4 family. *Toxicon* **45:**431–442.

Address correspondence to: Dr. Michael J. Morales, Department of Physiology and Biophysics, University at Buffalo, The State University of New York, 124 Sherman Hall, Buffalo, NY 14214. E-mail: moralesm@buffalo.edu